Rare Metal Materials and Engineering
Volume 49, Issue 7, July 2020
Available online at www.rmme.ac.cn

Science Press

Cite this article as: Rare Metal Materials and Engineering, 2020, 49(7): 2305-2313

ARTICLE

Hot Deformation Behavior and Dynamic Precipitation in Al-Er-Zr Alloy

Yuan Xiaoming, Wen Shengping, Hou Jie, Wu Xiaolan, Li Bolong, Gao Kunyuan, Huang Hui, Nie Zuoren

Beijing University of Technology, Beijing 100124, China

Abstract: The hot deformation behavior of Al-0.04Er-0.08Zr alloy was investigated by hot compression tests in the temperature range from 200 °C to 450 °C. True stress-true strain curves were analyzed by linear fitting using Arrhenius-type equation, and deformation microstructure was studied by TEM. The results indicate that dynamic recovery is the dominated softening mechanism for both the solutionized and the aged sample during hot compression. Hot deformation especially at high temperature and low strain rate induces rapid precipitation in the solutionized samples. Dynamic precipitation apparently leads to the increase of the flow stress of the solutionized samples during hot compression process, but does not effectively enhance the microhardness of the deformed samples. The dynamic precipitation also leads to deviations of the Arrhenius-type fitting of the stress-strain curves.

Key words: aluminum alloy; hot compression; dynamic precipitation; Erbium; Zirconium

Intensive researches have been conducted on micro-alloyed aluminum alloys, and researchers found that coherent intermetallic dispersoids with $L1_2$ structure are effective on strengthening and enhancement of the thermal stability in aluminum alloys[1]. During aging or homogenization process, the supersaturated Al-Zr alloys decompose to form a large amount of thermodynamically metastable, coherent, $L1_2$-structured Al_3Zr dispersoids which were thermally stable at elevated temperature[2,3]. These nano-scaled Al_3Zr dispersoids were resistant to coarsening and dissolution attributed to the low diffusivity of Zr in α-Al[1,4]. Therefore, small addition of Zr were often made to wrought high strength aluminum alloys to form Al_3Zr dispersoids which could inhibit recrystallization and control the evolution of grain and subgrain structures during hot rolling or solution treatment process[5]. But the precipitation kinetics of Al_3Zr was relatively sluggish due to the low diffusivity of Zr[6]. The strengthening effect of the dispersoids depended on the number density, size, volume fraction, inter-precipitate spacing and distribution[1]. For aluminum alloys micro-alloyed with Zr after aging, a gradient of dispersoids size and number density existed due to the dendritic micro-segregation of Zr during solidification[3,7], which had deleterious effects on the mechanical properties[2,8]. Moreover, the Al-Zr alloy could not be homogenized because the $D0_{23}$-structured Al_3Zr dispersoids precipitated in dendritic core reduced the amount of Zr available for precipitation in subsequent aging process[9].

Composite addition of Sc, Er or Yb combined with Zr can strengthen the alloy significantly by accelerating the precipitation process and increasing the number density of dispersoids due to the formation of core-shell structured dispersoids with Sc, Er or Yb segregated in the core and Zr in the shell[6, 10-13]. Silicon also had some influence on enhancing the precipitation kinetics in aluminum alloys such as Al-Hf, Al-Sc-Zr and Al-Sc-Er-Zr[14-16]. However, the aging time to obtain the peak hardness is still much longer than that of other age hardenable aluminum alloys. It had been reported

Received date: July 15, 2019
Foundation item: National Key Research and Development Program of China (2016YFB0300801, 2016YFB0300804)
Corresponding author: Wen Shengping, Ph. D., Associate Professor, School of Material Science and Engineering, Beijing University of Technology, Beijing 100124, P. R. China, E-mail: wensp@bjut.edu.cn

that dislocations and substructures introduced by deformation lead to a significant acceleration in precipitation process because of denser nucleation of dispersoids compared with static precipitation and higher diffusivities of solutes due to the dislocation pipe diffusion mechanism [17,18] in many kinds of alloys, such as steel and aluminum alloys[19,20]. These strain-induced dispersoids may in turn retard the recovery and recrystallization process by inhibiting dislocation and grain boundary movement[21,22], so as to preserve many substructures to improve the mechanical properties [23,24].

Previous research has shown that there is a synergetic effect between Er and Zr on the precipitation hardening of Al-Er-Zr alloys, which leads to a significant aging hardening effect by the addition of 0.04at% Er in Al-0.08Zr (at%) alloy. A large amount of nano-scaled, dispersed distributed and heat-resistant Al_3(Er, Zr) dispersoids form even at elevated temperature during aging[12], which indicates that Al_3(Er, Zr) dispersoids can be dynamically precipitated during hot deformation. However, there is no report on the dynamic precipitation in Al-Er-Zr alloys. Therefore, this paper investigates the dynamic precipitation behavior in this alloy and also the effect on mechanical properties.

1 Experiment

The experimental materials were prepared by diluting commercially pure aluminum with Al-6Er (wt%) and Al-4Zr (wt%) master alloys. Appropriate amount of the starting materials were melted by heating to 780 °C. The melt was cooled to about 720 °C, and then poured into an iron mold at room temperature to produce a 15 mm×150 mm×200 mm plate. The chemical composition was verified by X-ray fluorescence spectroscopy as shown in Table 1. For convenience, the nominal composition, Al-0.04Er-0.08Zr, was used to denote the alloys in the following text. Two kinds of samples denoted as solutionized and aged samples were prepared for subsequent hot compression test. The solutionized samples were homogenized in air at 640 °C for 20 h, then quenched in water to room temperature, while the aged samples were then isothermally aged at 350 °C for 65 h to reach the peak hardness.

Cylindrical samples for compression with 15 mm in length and 10 mm in diameter were machined from the solutionized and aged samples[25]. Hot compression tests were carried out on a Gleeble-3800 thermomechanical simulator at constant strain rates of 0.001, 0.01, 0.1, 1 and 10 s^{-1} with the temperature of 200, 300, 400 and 450 °C. The samples were padded with slices of graphite between samples and compression strokes for lubrication. All the samples were heated to test temperature with heating rate of 10 °C/s and held for 60 s to ensure temperature uniformity before compression. Each sample was deformed to a true strain of 0.6 and then water quenched to freeze the microstructure. The true stress-true strain data were obtained by the controlling computer with an automatic data acquisition system.

The compressed samples were sectioned parallel to the compression axis and polished for microhardness test. Vickers microhardness was measured by the mean value from at least 10 independent measurements with a load of 200 g and a dwell time of 10 s. Slices for transmission electron microscopy (TEM) samples were cut from the deformed samples parallel to the compression axis, and were subsequently ground to less than 70 μm and punched into 3 mm discs. Then thin foils for TEM observation were prepared by twin-jet polishing with an electrolyte solution consisting of 30% HNO_3 and 70% methanol below –30 °C. TEM observation was carried out by a JEOL 2010 microscope with an operating voltage of 200 kV.

2 Results and Discussion

2.1 True stress-true strain curves

Fig.1 shows the true stress-true strain curves with friction and temperature correction for Al-0.04Er-0.08Zr alloys compressed at temperatures from 200 °C to 450 °C with various strain rates from 0.001 to 10 s^{-1}[26]. Generally, the effects of temperature and strain rate on flow stress are significant. It can be seen that at the initial stage of compression, the flow stress rises sharply as strain increases due to work hardening, and then increases gradually with a relative low rate with growing strain. At a constant temperature the flow stress rises with the increase of strain rate, and at a constant strain rate the flow stress decreases with the increase of temperature. As can be seen from Fig.1, the flow curves exhibit monotonic hardening to a steady stage under the conditions of 400 °C/0.001 s^{-1}, 450 °C/ 0.001~0.1 s^{-1} for solutionized samples, and 400 °C/0.001 s^{-1}, 450 °C/ 0.001~0.01 s^{-1} for aged samples. At other conditions, however, the flow curves exhibit continuous flow increasing. The fault stacking energy of aluminum alloys is relatively high, which means that obstacles are easy to be overcome by dislocation movements through climb or cross-slip, and dynamic recovery is prone to occur during hot deformation. At high temperature and low strain rate, the curves exhibit steady stage as a result of balance between work hardening and dynamic softening, and dynamic recovery is the dominated mechanism, whereas at other conditions, work hardening is the dominated mechanism which consists of dislocation interaction and the rise of dislocation density [27-29].

Fig.2 shows the flow stress with true strain of 0.5 at different strain rates and temperature for both solutionized and aged samples[30]. For hot compression at 200 °C at the same strain rate, the flow stress of the aged samples is higher

Table 1 Chemical composition of the experimental alloy (at%)

Sample	Er	Zr	Si
Al-0.04Er-0.08Zr	0.031	0.085	0.140

than that of the solutionized samples. However, at temperature of 300 °C and strain rate of 0.001 s^{-1}, the flow stress of the solutionized sample is higher than that of the aged sample. At temperature of 400 and 450 °C, the flow stress of the solutionized sample is higher than that of the aged sample at strain rate which ranges from 0.001 s^{-1} to 1 s^{-1}. The solutionized samples were homogenized in air at 640 °C for 20 h and quenched in water to room temperature before hot compression, i.e. solution treatment for Al-Er-Zr alloy. Therefore, no Al_3(Er, Zr) secondary dispersoids existed in the solutionized samples before compression. The aged samples were isothermally aged at 350 °C for 65 h to approach the peak hardness before compression, and this resulted in the precipitation of Al_3(Er, Zr) dispersoids which were dispersed distributed in Al matrix with high number density and small size[12]. These nano-scaled dispersoids inhibit the dislocation movements, which should lead to the larger deformation resistance in most cases. But there are exceptions as shown in Fig.2. Further investigations have been made below to study this phenomenon.

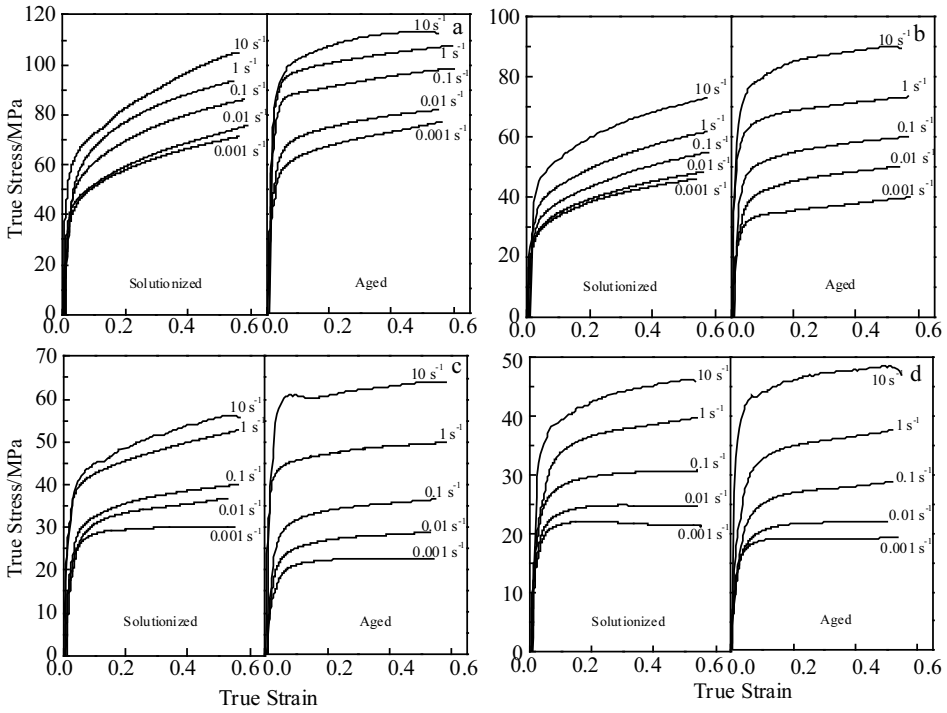

Fig.1 True stress-true strain curves of solutionized and aged samples for Al-Er-Zr alloys at different temperatures: (a) 200 °C, (b) 300 °C, (c) 400 °C, and (d) 450 °C

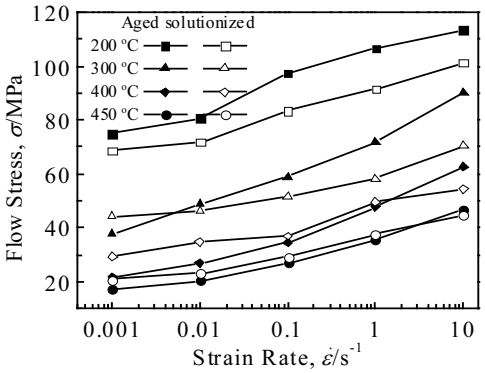

Fig.2 Flow stress with true strain of 0.5 at different strain rates and temperatures for both solutionized and aged samples

2.2 Linear fitting analyses

When aluminum alloys are deformed at elevated temperature, work hardening and dynamic restoration occur contemporarily, and flow curves are the result of interaction of them. Dynamic recovery and dynamic recrystallization are the two softening mechanisms during hot deformation process in alloys, which concurrent and compete with each other[28], and for aluminum alloys dynamic recovery is prone to occur. Generally the correlation between flow stress and work conditions can be established by analyzing flow curves. A hyperbolic-sine Arrhenius-type equation has been widely used to describe the relationship among strain rate ($\dot{\varepsilon}$), flow stress (σ) and temperature (T) during hot deformation [28,31]:

$$\dot{\varepsilon} = A[\sinh(\alpha\sigma)]^n \exp(-Q/RT) \quad (1)$$

where Q is the deformation activation energy, R is the gas constant, σ is the flow stress, A, α and n are materials con-

stants. When the flow stress is low, Eq.(1) can be simplified to a power relationship similar to that for creep:

$$\dot{\varepsilon} = A'\sigma^{n'}\exp(-Q/RT) \quad (2)$$

while at high stress, Eq.(1) becomes an exponential relationship:

$$\dot{\varepsilon} = A''\exp(\beta\sigma)\exp(-Q/RT) \quad (3)$$

$$\alpha = \beta/n' \quad (4)$$

where A', A'', n', β are materials constants.

Supposing that the relationship between flow stress and work conditions of the tested alloy satisfies Eq.(1) to Eq.(3), the following equations can be obtained by taking the logarithm of both sides of the three equations:

$$\ln\dot{\varepsilon} = \ln A + n\ln[\sinh(\alpha\sigma)] - Q/RT \quad (5)$$

$$\ln\dot{\varepsilon} = \ln A' + n'\ln\sigma - Q/RT \quad (6)$$

$$\ln\dot{\varepsilon} = \ln A'' + \beta\sigma - Q/RT \quad (7)$$

Substituting the values of strain rates and corresponding flow stresses at the true strain of 0.5 into Eq.(6) and Eq.(7) gives the relationship between flow stress and strain rate at different temperatures, as shown in Fig.3. According to Eq.(7), a linear relationship exists between $\ln\dot{\varepsilon}$ and σ with slope β, and for Eq.(6) a linear relationship exists between $\ln\dot{\varepsilon}$-$\ln\sigma$ and $\ln\dot{\varepsilon}$ with slope n'. The values of β and n' can be obtained from the slope of each line in $\ln\dot{\varepsilon}$-σ and $\ln\dot{\varepsilon}$-$\ln\sigma$ plots by linear fitting as shown in Fig.3. The mean value of β and n' for solutionized samples can be computed as 0.3217/MPa and 16.8702, and for aged samples are 0.2290/MPa and 12.5117, respectively. Then α for solutionized alloy is 0.0191/MPa and for aged alloy is 0.0183/MPa.

The values of n can be obtained from the slope of each line in $\ln\dot{\varepsilon}$-ln[sinh($\alpha\sigma$)] plots by linear fitting. The $\ln\dot{\varepsilon}$ and ln[sinh($\alpha\sigma$)] of the aged samples show a good linear relationship with slopes n of 8.2, 7.5, 7.7 and 7.0 at 200, 300, 400 and 450 °C, respectively as indicated by Fig.4b, but there are apparent deviations for solutionized samples at 400 and 450 °C as shown in Fig.4a. The deviations are the most remarkable at the strain rate of 0.001 and 0.01 s^{-1}, i.e. at high temperature and low strain rate. For solutionized samples the slopes at 200 and 300 °C are 16.2 and 15.0, respectively. At 400 and 450 °C, the slopes at the strain rates between 0.1 and 10 s^{-1} are 11.1 and 10.4, respectively. In contract, at the lower strain rates between 0.001 and 0.1 s^{-1}, the slopes of the curves at 400 and 450 °C are 6.6 and 6.5, respectively, which are lower than that at higher strain rate and lower temperatures but close to that of the aged samples.

Another linear relationship can be derived from Eq.(5) and simplified as Eq.(8). The slopes can be derived by partial differentiating and expressed as Eq.(9). Substituting the values of temperatures and corresponding flow stresses at the true strain of 0.5 into Eq.(8) gives the plots of ln[sinh($\alpha\sigma$)]-1000/T, and the values of the slopes can be obtained by linear fitting, as shown in Fig.3.

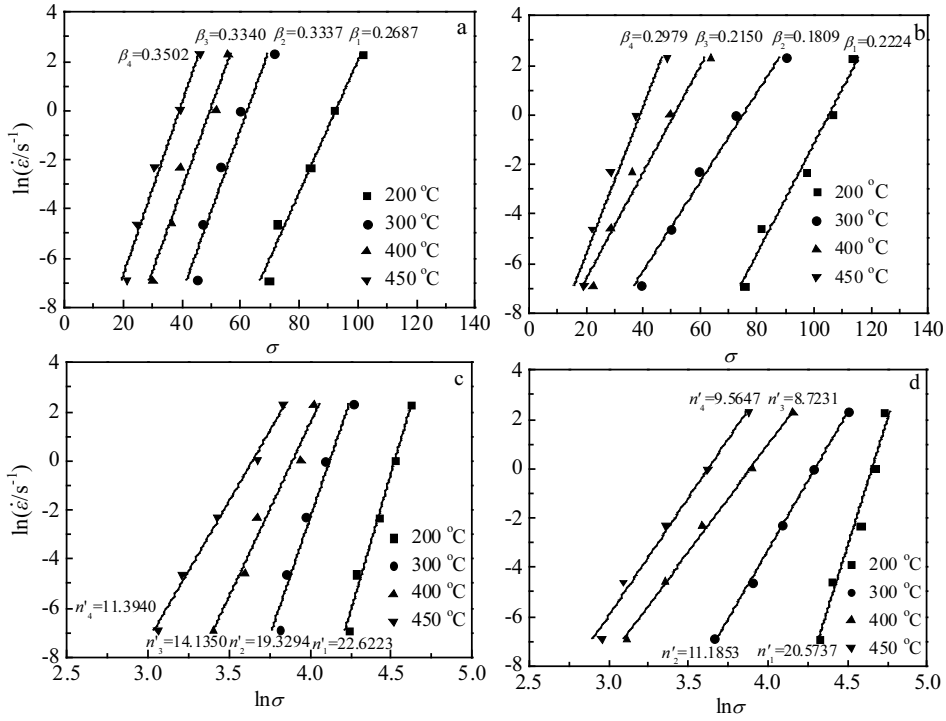

Fig.3 Relationships of $\ln\dot{\varepsilon}$-σ for solutionized (a) and aged (b) samples; $\ln\dot{\varepsilon}$-$\ln\sigma$ for solutionized (c) and aged (d) samples

$$\ln[\sinh(\alpha\sigma)] = \frac{Q}{nR}\frac{1}{T} + \frac{\ln\dot{\varepsilon} - \ln A}{n} \quad (8)$$

$$\frac{Q}{nR} = [\frac{\partial \ln[\sin h(\alpha\sigma)]}{\partial(1/T)}]_{\dot{\varepsilon}} \quad (9)$$

For the linear relationship between ln[sinh($\alpha\sigma$)] and 1000/T, aged samples show a good linear relationship with slopes of 2.5, 2.5, 2.6, 2.6 and 2.2 at the strain rate of 0.001, 0.01, 0.1, 1 and 10 s^{-1}, respectively as indicated by Fig.4d, but there are apparent deviations for solutionized samples at the strain rate of 0.001 and 0.01 s^{-1} as shown in Fig.4c. The slopes of the curves of solutionized samples at the stain rate of 0.1 and 1 and 10 s^{-1} are 1.6, 1.6 and 1.5, respectively. At the strain rate of 0.001 and 0.01 s^{-1}, the slopes between 200 and 300 °C are 1.6 and 1.5, respectively, which are similar to the slopes at high strain rates. However, the slopes between 300 and 450 °C are 3.2 and 3.1, which are greater than that at higher strain rates and lower temperatures but close to that of the aged samples as shown in Fig.4c.

2.3 Microstructure observation

Fig.5 shows the microstructures of solutionized samples compressed at 200, 400 °C and at a strain rate of 0.001 s^{-1}. As can be seen from Fig.5a and 5b，there exist so many subgrains at both 200 °C and 400 °C, which implies that dynamic recovery coexists with the deformation.

Fig.6 shows the microstructures of solutionized samples compressed at 200, 300, 400 and 450 °C at a strain rate of 0.001 s^{-1}. It can be seen from Fig.6a and 6b that there is no observable dispersoids no matter in subgrains or at the sub grain boundaries at 200 and 300 °C. At 400 °C, however,

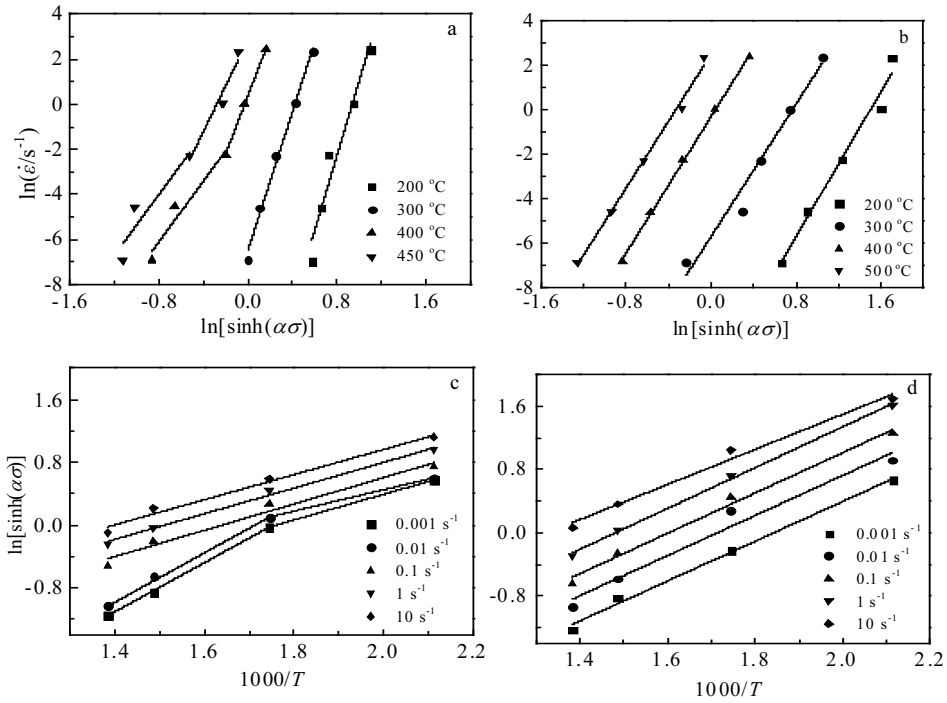

Fig.4 Relationships of $\ln\dot{\varepsilon}$-ln[sinh($\alpha\sigma$)] for solutionized (a) and aged samples (b); ln[sinh($\alpha\sigma$)]-1000/T for solutionized (c) and aged samples (d)

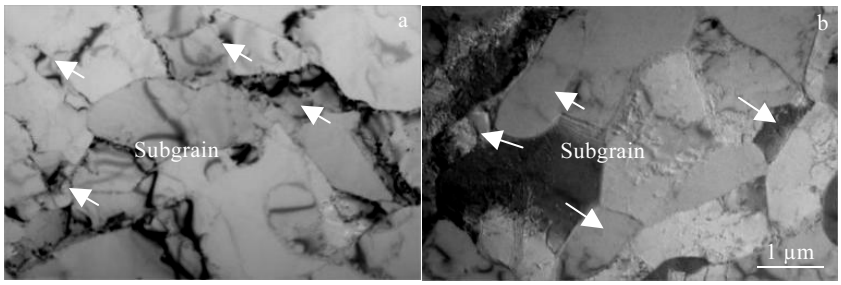

Fig.5 TEM images of the solutionized samples after hot compression with a strain rate of 0.001 s^{-1} at temperatures of 200 °C (a) and 400 °C (b)

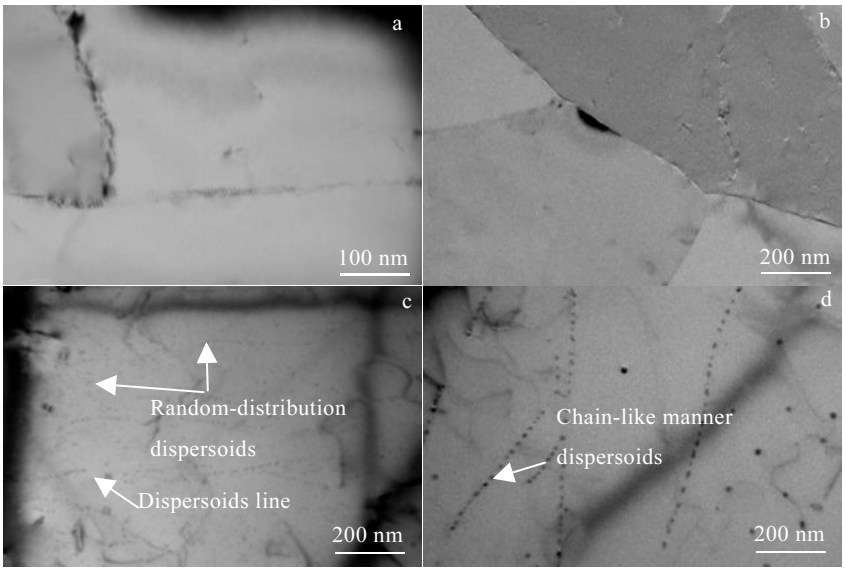

Fig.6 TEM images of the solutionized samples after hot compression at different temperatures with a strain rate of 0.001 s^{-1}: (a) 200 °C, (b) 300 °C, (c) 400 °C , and (d) 450 °C

there are great amounts of nano-scaled dispersoids, and the distribution is not homogeneous. Some dispersoids distribute along a line, while others distribute relatively dispersively as shown in Fig.6c. At 450 °C there are also many dispersoids and the distribution is also heterogeneous similar to 400 °C as shown in Fig.6d. The nano-scaled dispersoids heterogeneously distributed in a chain-like manner imply that they are nucleated on dislocations or substructures introduced by hot compression.

Fig.7 shows the microstructure of solutionized samples after hot compression at 400 °C with strain rates of 0.01~10 s^{-1}. From Fig.7a it can be found that there are large amounts of dispersoids after compression with strain rate of 0.01 s^{-1}. Fig.7b~7d are the microstructure of the samples compressed with strain rates of 0.1, 1 and 10 s^{-1}, respectively. In Fig.7b there still exist many dispersoids, but the number density decreases apparently compared with Fig.7a, and most of the dispersoids distribute along lines. In Fig.7c and 7d, with the increase of strain rate, the number density decreases further, while the proportion of the linear distributed dispersoids increases. At the strain rate of 10 s^{-1} a few dispersoids exist and almost all of them distribute in a chain-like manner as shown in Fig.7d.

As concluded from Fig.6 and Fig.7, high temperature and low strain rate is suitable for dynamic precipitation in Al-0.04Er-0.08Zr alloy. The dynamic precipitation is significantly affected by hot compression temperature. As shown in Fig.6, there are many dispersoids after compression at 400 °C and 450 °C with strain rate of 0.001 s^{-1}, and most of them nucleate on dislocations. At 200 °C and 300 °C, however, few dispersoids appear in the samples compressed at the same strain rate of 0.001 s^{-1} (i.e. the longest deformation time). This is due to the fact that the diffusivities of Er and Zr in α-Al increase exponentially with increase of temperature. For this reason, the dynamic precipitation is sluggish at 200 and 300 °C even though accelerated by dislocations and thereby cannot retard the dislocation movements effectively contrast to that at 400 and 450 °C.

Dynamic precipitation is also affected by strain rate when the sample is deformed at constant temperature. With the increase of strain rate, the number density of dispersoids declines, and the proportion of the heterogeneously distributed dispersoids increases at 400 °C as shown in Fig.7. The possible reason is that with the increase of strain rate, the time for deformation and precipitation becomes shorter, which means that less time is available for the dispersoids to grow and coarsen. The dispersoids tend to nucleate on defects such as dislocations because heterogeneous nucleation reduces the nucleation energy, while the growth and coarsening rates increase due to the dislocation pipe diffusion mechanism[17]. Therefore, at high strain rate only the dispersoids nucleated on dislocations have enough time to grow and coarsen to the size observable in TEM, which leads to the more inhomogeneous distribution of dispersoids.

It has been well known that the precipitation can occur at a rate considerably larger than static precipitation when deformation is continuous and concurrent with the precipitation. This is attributed to the dense nucleation on dislocations and enhanced growth rate under the deforming conditions[19,20]. According to previous research, it took several hours to obtain observable dispersoids in TEM when iso-

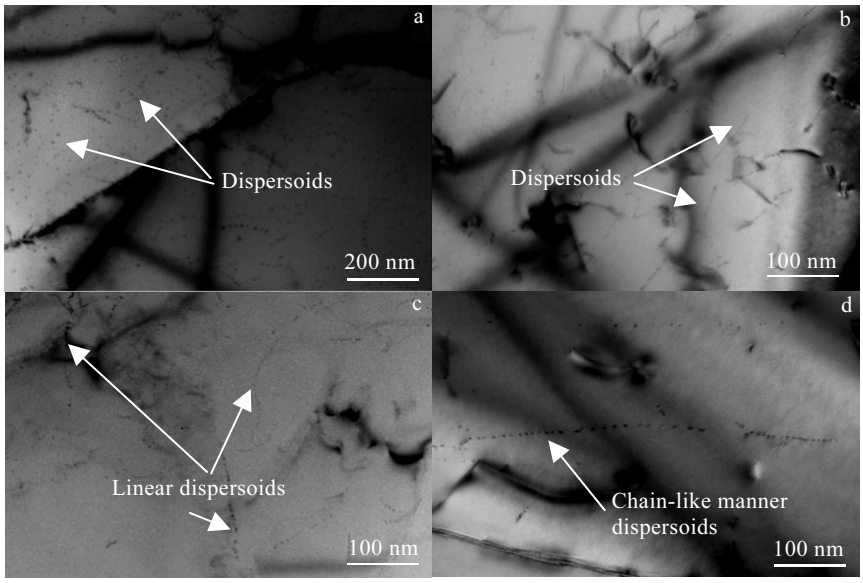

Fig.7 TEM images of the solutionized samples after hot compressed at 400 °C with different strain rates: (a) 0.01 s^{-1}, (b) 0.1 s^{-1}, (c) 1 s^{-1}, and (d) 10 s^{-1}

thermally aged at 400 °C[13]. In this study, there are observable dispersoids after being compressed within one minute (with strain rate of 1 s^{-1}), and the number density of dispersoids is relatively high after being deformed at a strain rate of 0.001 s^{-1} (for 10 min) at 400 °C. This reveals that hot deformation induces the rapid precipitation in Al-0.04Er-0.08Zr alloy.

2.4 Influence of dynamic precipitation on mechanical properties

In order to investigate the influence of dynamic precipitation on the mechanical properties for Al-Er-Zr alloy, flow curves and microhardness of the solutionized and aged samples were compared. The microhardness values of the two kinds of samples after compression are shown in Table 2. It is easy to find that the values of microhardness for aged samples are significantly larger than those of solutionized samples at all the compression conditions in this research. For aged samples, referring to the TEM images for Al-0.04Er-0.08Zr alloy isothermally aged at 350 °C for 65 h in previous research[12], there are a great amount of small-sized, dispersed distributed Al_3(Er, Zr) dispersoids in the Al matrix before compression. As shown in Fig.6 and Fig.7, for solutionized samples compressed at 400 °C and 450 °C, the sizes of dispersoids are larger because of the enhanced growth and coarsening rates, the distribution is not homogeneous because of heterogeneous nucleation, and the volume fraction is lower due to the very short deforming time. Therefore, these strain induced dispersoids cannot strongly retard the dislocation movements at room temperature compared to those static-precipitated dispersoids in aged samples. And there is even no observable dispersoids in the samples after they are compressed at 200 °C and 300 °C. These result in the lower microhardness for as-deformed solutionized samples.

According to the results of the linear analysis, aged samples fit the linear relationships well but not for solutionized samples. During hot deformation process, dynamic precipitation may occur in both the solutionized and aged samples. For aged samples, peak hardness has been nearly approached by previous aging, which leads to the low supersaturation of solutes in α-Al matrix and thus results in low driving force for the subsequent precipitation of Al_3(Er, Zr) dispersoids[3]. Therefore, the dynamic precipitation is not strong enough to significantly affect the flow behavior and the linear relationships.

For solutionized samples, many Al_3(Er, Zr) dispersoids appeared on dislocations by means of dynamic precipitation during hot compression. As mentioned in Section 2.1 and 2.2, when the samples are deformed at 400 °C and 450 °C with strain rates of 0.001~1 s^{-1}, the flow stress of solutionized samples are higher than that of the aged samples, and the deviations to linear relationships appear at the strain rates of 0.001~0.01 s^{-1}. The mechanisms of this phenomenon are below: (1) For solutionized samples, dynamic precipitation on dislocations and substructures significantly enhance the deformation resistance by strongly dragging and pinning the dislocation movements. In particular, at the low strain rates, it has longer time for solutionized samples to form enough dynamic-precipitated dispersoids thus leading to the significant deviations to linear relationships. (2) The sizes of the dispersoids are larger than those of aged samples, which may retard the dislocation climb and cross-slip more effectively

than the dispersoids in aged samples. (3) Micro-alloying elements atoms or the formation of atomic cluster may also retard the dislocation movements during hot compression[32]. These mechanisms also give the explanation of the higher average hot deformation activation energy for the solutionized samples than for the aged samples.

Generally, for solutionized samples the diffusivities of solute atoms are too low at 200 °C and 300 °C, while the deformation time is too short at 400 °C and 450 °C with $\dot{\varepsilon}$>1 s^{-1} to form enough dynamic-precipitated dispersoids to potently retard the dislocation movements. And this leads to the lower flow curves compared with aged samples. However, at the condition of 300 °C/0.001 s^{-1}, there are no dispersoids observable in the compressed solutionized sample as shown in Fig.5b, but the flow curve is still higher than that of the aged sample. It is possible that there exist some dispersoids which are too small to be observed due to the low diffusivities of Er and Zr atoms, but these strain induced dispersoids can also retard the dislocation movements effectively during compression.

Table 2 Vickers microhardness values (HV) of solutionized and aged samples after hot compression (MPa)

Samples	Temperature/°C	Strain rates, $\dot{\varepsilon}$ /s^{-1}				
		0.001	0.01	0.1	1	10
Solutionized	200	433	435	431	426	430
	300	399	403	414	407	413
	400	338	342	364	424	395
	450	326	338	343	341	358
Aged	200	576	552	577	582	627
	300	578	595	557	569	583
	400	533	508	576	528	539
	450	516	558	547	574	561

3 Conclusions

1) Dynamic recovery is the main restoration mechanism during hot compression for both aged and solutionized samples at temperature ranging from 200 to 450 °C with strain rate from 0.001 s^{-1} to 10 s^{-1}. The linear fitting of the flow curves of the solutionized samples show a deviation because of dynamic precipitation which affect deformation behavior by retarding dislocation and subgrain boundary movements during hot compression process, especially at 400 °C and 450 °C with strain rate of 0.001 $s^{-1}$and 0.01 s^{-1}.

2) Hot compression accelerates precipitation in solutionized Al-0.04Er-0.08Zr alloys. There are observable precipitates after deformation with strain rate of 1 s^{-1}(within one minute), and the number density of precipitates is relatively high after deformation with strain rate of 0.001 s^{-1}(for 10 min). However, there are few precipitates after hot deformation at 200 °C and 300 °C because of low diffusivity of Er and Zr.

3) The flow stress of the solutionized samples are close to that of the aged samples at high temperature and low strain rate mainly because dynamic precipitation retards dislocation movement effectively during hot compression process, which enhances hot deformation resistance. But the microhardness of the solutionized samples is lower than that of the aged samples after compression.

References

1 Knipling K E, Dunand D C, Seideman D N. *Z Metallkd*[J], 2006, 97: 246

2 Knipling K E, Dunand D C, Seidman D N. *Acta Materialia*[J], 2008, 56(6): 1182

3 Knipling K E, Dunand D C, Seidman D N. *Metallurgical & Materials Transactions A*[J], 2007, 38(10): 2552

4 Booth-Morrison C, Dunand D C, Seidman D N. *Acta Materialia*[J], 2011, 59(18): 7029

5 Robson J D, Prangnell P B. *Acta Materialia*[J], 2001, 49(4): 599

6 Knipling K E, Karnesky R A, Lee C P *et al*. *Acta Materialia*[J], 2010, 58(15): 5184

7 Dalen M E V, Dunand D C, Seidman D N. *Acta Materialia*[J], 2005, 53(15): 4225

8 Knipling K E, Dunand D C. *Scripta Materialia*[J], 2008, 59(4): 387

9 Knipling K E,Seidman D N, Dunand D C. *Acta Materialia*[J], 2011, 59(3): 943

10 Tolley A, Radmilovic V, Dahmen U. *Scripta Materialia*[J], 2005, 52(7): 621

11 Zhang Y, Zhou W, Gao H *et al. Scripta Materialia*[J], 2013, 69(6): 477

12 Wen S P, Gao K Y, Li Y *et al. Scripta Materialia*[J], 2011, 65(7): 592

13 Huang H,Wen S P, Gao K Y *et al*. *Metallurgical and Materials Transactions A*[J], 2013, 44(6): 2849

14 Booth-Morrison C, Mao Z, Diaz M *et al*. *Acta Materialia*[J],

2012, 60(12): 4740
15 Hallem H, Forbord B, Marthinsen K. *Materials Science & Engineering A*[J], 2004, 387-389: 940
16 Vo N Q, Dunand D C, Seidman D N. *Acta Materialia*[J], 2014, 63(3): 73
17 Chen J, Tang S, Liu Z *et al*. *Journal of Materials Science*[J], 2012, 47(11): 4640
18 Dutta B, Palmiere E J, Sellars C M. *Acta Materialia*[J], 2001, 49(5): 785
19 Weiss I, Jonas J J. *Metallurgical Transactions A*[J], 1979, 10(7): 831
20 Cécile G, Damien F, Deschamps A *et al*. *Materials Science & Engineering A*[J], 2006, 441(1-2): 39
21 Jones M J, Humphreys F J. *Acta Materialia*[J], 2003, 51(8): 2149
22 Hansen S S, Sande J B V, Cohen M. *Metallurgical and Materials Transactions A*[J], 1980, 11(3): 387
23 Lang Y, Cai Y, Cui H *et al*. *Materials and Design*[J], 2011, 32(8-9): 4241
24 Singh S, Goel D B. *Journal of Materials Science*[J], 1990, 25(9): 3894
25 Ebrahimi R, Najafizadeh A. *Mater Process Techno*[J], 2004, 152: 136
26 Ningqi P, Guangbo T, Zhengdong L. *Hot Working Technology*[J], 2012, 41(17): 20
27 Jeswieta J, Geiger M, Engel U. *CIRP Journal of Manufacturing Science and Technology*[J], 2008, 1(1): 2
28 Gourdet S, Montheillet F. *Materials Science and Engineering A*[J], 2000, 283(1-2): 274
29 Ashtiani H R R, Parsa M H, Bisadi H. *Materials Science & Engineering A*[J], 2012, 545: 61
30 Monajati H,Taheri A K, Jahazi M *et al. Metallurgical and Materials Transactions A*[J], 2005, 36(4): 895
31 Sellars C M, Mctegart W J. *Acta Metallurgica*[J],1966, 14(9): 1136
32 Andrade H L, Akben M G , Jonas J J. *Metallurgical Transactions A*[J],1983, 14(10): 1967

Al-Er-Zr 合金的热变形行为及动态析出

袁晓明，文胜平，侯 杰，吴晓蓝，李伯龙，高坤元，黄 晖，聂祚仁
(北京工业大学，北京 100124)

摘 要：通过200~400 ℃温度范围内的热压缩实验对Al-0.04Er-0.08Zr的热变形行为进行了研究。通过实验得到的应力-应变曲线是利用Arrhenius-type方程线性拟合来分析的，合金的变形微观结构通过透射电镜进行观察。结果表明，不论是固溶态合金还是时效态合金在热压缩过程中其都是以动态回复为主要软化恢复机制。固溶态合金样品在高温以及低应变速率的热压缩条件下会发生快速时效析出，且动态析出会明显增加固溶态合金在热压缩过程中表面受到的流变应力，但并不能有效地提高变形合金的硬度。动态析出还会导致应力-应变曲线在运用Arrhenius-type方程线性拟合时出现一定的偏差。

关键词：铝合金；热压缩；动态析出；铒；锆

作者简介：袁晓明，男，1993 年生，硕士生，北京工业大学材料科学与工程学院，北京 100124, E-mail: stanfordyuan@163.com